OPEN ACCESS
IOP Publishing
Smart Materials and Structures
Smart Mater. Struct. **33** (2024) 085040 (14pp)
https://doi.org/10.1088/1361-665X/ad6414

Tailoring the stress-free two-way shape memory effect in sol–gel crosslinked poly(ε-caprolactone)-based semicrystalline networks

Nicoletta Inverardi[1,5,6,*], Maurizio Toselli[2,5], Massimo Messori[3,5], Giulia Scalet[4,5], Ferdinando Auricchio[4,5] and Stefano Pandini[1,5]

[1] Department of Mechanical and Industrial Engineering, University of Brescia, via Branze 38, 25133 Brescia, Italy
[2] Department of Industrial Chemistry 'Toso Montanari', University of Bologna, Viale Risorgimento 4, 40136 Bologna, Italy
[3] Department of Applied Science and Technology, Politecnico di Torino, Corso Duca degli Abruzzi 24, 10129 Torino, Italy
[4] Department of Civil Engineering and Architecture, University of Pavia, via Ferrata 3, 27100 Pavia, Italy
[5] INSTM, National Interuniversity Consortium of Materials Science and Technology, 50121 Firenze, Italy

E-mail: ninverardi@mgh.harvard.edu

Received 19 April 2024, revised 6 June 2024
Accepted for publication 16 July 2024
Published 25 July 2024

Abstract

Two-way shape memory polymers are stimulus-responsive materials capable of changing their shape between two configurations based on an on/off thermal stimulus. While the traditional effect has been studied under the application of an external mechanical load, it was demonstrated also in the absence of an external load. Such a response only relies on a carefully tailored macromolecular architecture of the polymer combined with a specific thermo-mechanical protocol. In particular, semicrystalline networks, either consisting of a multi-phase copolymer network or a homopolymer based network with broad phase transitions, have been proposed to this aim under ad hoc thermo-mechanical histories. In this work, the two-way shape memory behavior is studied on a poly(ε-caprolactone)-based network, crosslinked by means of a sol–gel approach and tailored on the selection of the molecular weight of the precursor polymer. Changing the prepolymer precursor allowed to tune the melting/crystallization regions of the networks, thus the thermal region of the reversible shape memory effect. The application of properly designed thermo-mechanical cycles allowed to study the two-way shape memory effect without the application of an external load under tensile conditions. Given a specific network, the stress-free actuation of the reversible elongation-contraction cycle under tensile conditions was induced across its specific melting/crystallization region. The extent of the effect was found to depend on the crystalline fraction remaining for the given actuation temperature and on the tensile stretched state imposed

[6] Present address: Harris Orthopaedics Laboratory, Massachusetts General Hospital and Department of Orthopedic Surgery, Harvard Medical School, 55 Fruit Street, Boston, MA 02114, United States of America.
[*] Author to whom any correspondence should be addressed.

on the materials during the training step. The results were compared with the response achieved under the traditional two-way shape memory protocol under stress. The stress-free two-way shape memory effect was also successfully demonstrated and emphasized, under flexural conditions, which suggests the potential of these materials as intrinsically reversible actuators, promising for applications in the biomedical field and/or for soft robotics.

Keywords: shape memory polymers, poly(caprolactone), two-way shape memory effect, stress-free reversible shape memory effect, crystallization, crosslinked networks

1. Introduction

Shape memory polymers (SMPs) are a class of stimulus-responsive materials which have drawn significant attention in the course of the years due to their great potential for many challenging applications in which an external, non-mechanical actuation of a device is required in several different fields, ranging from biomedical [1–4], aerospace [5] to robotics [6–9].

Their traditional response consists in the so-called 'one-way shape memory effect', which is a uni-directional change from a temporary shape to the permanent one, upon exposure to a triggering stimulus [10, 11].

Great research efforts were devoted to the investigation of several different triggering stimuli to be suitable for the different application needs, by way of example consisting of the exposure to heat, light, moisture, magnetic and electric fields, and thus to the synthesis of relevant material chemistries [12].

A challenge faced in order to tailor the response of SMPs on the specific intended application regarded the investigation of different effects other than the one-way, such as the temperature-memory effect, the multi-shape memory effect and the two-way shape memory effect [13–15]. In particular, the achievement of materials capable of reversibly switching between two shapes, as already obtained by their metallic counterparts, i.e. shape memory alloys, was intensively studied for applications in which the working principle relies on a repeated actuation, as in the case of actuators for soft robotics and artificial muscles [16, 17], and resulted in two-way SMPs.

For these materials, which consisted of semicrystalline networks, it was observed that, after a pre-stretch in tensile conditions, a significant elongation takes place when the polymer in its melt state is cooled under the presence of an applied stress (typically, above a hundred kPa) below its crystallization temperature. If thereafter the material is heated above its melting temperature under the applied load, it exhibits a contraction which almost completely recovers the previous elongation [18–20].

Several studies considered poly(caprolactone) (PCL)-based semicrystalline networks as model materials to investigate the effect because they inherently show very good one-way shape memory behavior [21, 22] and, PCL can be prepared starting by precursors of different molecular architectures, crosslinked under different chemical routes, blended with other polymers [23–25], and used for biomedical applications thanks to its biocompatibility [26].

The first work reporting the two-way shape memory effect for PCL was published in 2010 by Hong *et al* [19], early after the first identification of this reversible response for a crosslinked poly(cyclooctene) by Chung *et al* [18]. Hong *et al* reported that a PCL-based shape memory polyurethane, which is made of hard segments acting as crosslinks and of soft segments (i.e. PCL chains) composed of an amorphous phase and a crystallizable one, is capable of significant elongation under load. The proposed mechanism consisted in the alignment of the chains of the soft segment to the loading direction and the consequent oriented crystallization upon cooling under the constant force applied [19].

Soon after, Behl *et al* proposed for the first time the achievement of the so-called 'bidirectional' SMPs, i.e. SMPs capable of switching between two shapes under stress-free conditions along cooling/heating histories [16]. They synthesized multiphase copolyester urethane networks with two crystallizable units as model materials and identified the working mechanism of this effect. In fact, in experiments carried out under tensile conditions, they considered one crystalline phase responsible for the actuation, as cyclically promoting shrinkage upon heating above its melting temperature and elongation upon cooling below its crystallization temperature, and the other crystalline phase responsible for providing a skeleton and an internal driving force for the crystallization of the aforementioned actuator phase. Leveraging multiphasic semicrystalline networks was also shown in other works to be one of the potential strategies to obtain stress-free two-way shape memory effect [27–29]. Saatchi *et al* proved that this stress-free bidirectional shape memory effect, also referred to as 'self-standing' two-way shape memory effect, can be achieved also in semicrystalline polymer networks provided with a broad melting temperature range [27]. In this case, by employing a thermo-mechanical protocol, it was possible to select a so-called separation temperature, T_{sep}, and divide the melting area into two separate zones: a part for temperature lower than T_{sep}, which plays the role of the actuating phase that cyclically melts and crystallizes to promote macromechanical shrinkage/elongation; the other part, for temperature higher than T_{sep}, which acts as the skeleton domain, providing the internal force. In order to obtain a broad melting range, they used copolymer networks based on oligo(ε-caprolactone) and *n*-butyl acrylate (BA), whereas for the same aim, Yang *et al* synthesized networks based on different molecular weights of poly(ethylene glycol) and BA [30]. Interestingly, the self-standing two-way shape

memory effect based on the exploitation of a broad melting region was achieved also in monophasic polymeric networks, as demonstrated for a poly(octylene adipate)[31] and chemically crosslinked poly(ethylene-co-vinyl-acetate) [32–34]. Furthermore, also in crosslinked PCL, the occurrence of reversible shape-shifting under stress-free conditions was observed and ascribed by the authors to several mechanisms synergically working based on: (i) the oriented growth of crystals [35]; (ii) the introduction of built-in stresses deriving from a second curing performed on the stretched PCL structure [36]; (iii) an internal tensional force stemmed from the presence of dynamic reversible bonds [37]; and/or, as recently suggested, (iv) enhanced by a thermo-mechanical strategy to enable self-nucleated crystallization [38]. Noticeably, for this last method, the treated material is considered to be composed by annealed crystals, that are the unmelted crystals during annealing which undergo lamellar thickening, acting as the skeleton domain, and primary crystals, formed during cooling after annealing, which represent the actuation phase [38].

In a companion paper, the preliminary results on the shape-shifting capabilities of a sol–gel crosslinked PCL under stress-free conditions were demonstrated [39]. The excellent one-way shape memory capabilities (with strain fixity close to 100% and strain recovery greater than 90%) and stress-driven two-way shape memory behavior were also reported for these semicrystalline networks based on PCL precursors with different molecular weights, crosslinked by a sol–gel approach [24]. In these systems, an additional benefit is that crosslinking was achieved by mild reaction conditions, i.e. at room temperature and without the use of potentially toxic components such as organic peroxides and residual monomers typically used for free-radical thermal- or UV-curing. Based on these promising results, in this work we performed a thorough thermal, thermo-mechanical and shape memory characterization of these materials, with a special focus on their stress-free two-way shape memory behavior. The resulting materials showed tunable thermal properties, crystallinity content and crosslink density. The effect of these parameters on the self-standing two-way shape memory response was investigated and compared to results obtained under stress-driven conditions.

2. Materials and methods

2.1. Materials

Semicrystalline networks based on poly(ε-caprolactone) (PCL) of various molecular weights were obtained by crosslinking under mild conditions using a sol–gel approach, following a protocol described elsewhere [21, 24]. α,ω-hydroxyl-terminated PCL with different number-average molecular weights (i.e. 2200, 3400 and 10 000 g mol^{-1}, as measured by ^{1}H NMR), 3-(triethoxysilyl) propyl isocyanate (ICPTS), tetrahydrofuran (THF), ethanol (EtOH), water and hydrochloric acid (37%) were purchased from Sigma-Aldrich (Milan, Italy) and used as received without any further purification.

Briefly, the first step regarded the obtainment of α,ω-triethoxysilane-terminated precursors by reacting the α,ω-hydroxyl-terminated PCL with ICPTS, added with a 20% stoichiometric excess with respect to hydroxyl groups of PCL, in bulk at 130 °C for 2 h under nitrogen atmosphere and magnetic stirring. Afterwards, a solution of the α,ω-triethoxysilane-terminated precursors was prepared in THF with a 1:2 weight ratio and by adding EtOH to favor miscibility, water for the hydrolysis reaction, and HCl at a EtO:EtOH:H2O:HCl = 1:1:1:0.01 molar ratio with respect to the ethoxide groups of the modified PCL. The solution was then poured into a mold made by a Petri dish and covered with a plastic sheet to ensure slow solvent evaporation before gelation. After a few hours at room temperature for the gelation to complete, further entrapped solvent and other volatile products were let to evaporate and eventually the samples were obtained as thin circular sheets (thickness about 200–500 μm; diameter about 140 mm). The materials were coded as PCLSG 2, PCLSG 3, PCLSG 10, in which 2, 3 or 10 refer to the initial molecular weight of the precursor, 2200, 3400 or 10 000 g mol^{-1}, respectively. The initials 'SG' stands for sol–gel crosslinked, indicating that the gelation occurred due to the formation of crosslinked silica domains. PCLSG 2 was also prepared in a tubular shape with thin walls (height of 40 mm, outer diameter of 25 mm and wall thickness of 1–1.5 mm) by pouring the solution into silicon molds, as described in details elsewhere [26].

2.2. Physical and thermo-mechanical characterization of the materials

Swelling experiments were carried out by placing the samples ($30 \times 6 \times 0.2$ mm^3) cut from the casted sheets, with an initial mass, m_0, inside 20 ml of THF at room temperature. At least, three samples for each material were used to ensure repeatability of the measurement. After 24 h, the samples were removed from the solvent and the mass of the swollen specimens at equilibrium, m_s, was measured. Then, the samples were dried at room temperature under hood until constant weight to determine the residual mass after extraction, m_d.

The degree of swelling of the organic phase (Q) and the gel content (G) were calculated according to the following equations:

$$Q = 1 + \frac{\rho_1}{\rho_2}\left(\frac{m_s}{m_d} - 1\right) \tag{1}$$

$$G = \frac{m_d}{m_0} \tag{2}$$

where ρ_1 is the density of THF (equal to 0.889 g cm^{-3}) and ρ_2 is the density of PCL (equal to 1.094 g cm^{-3}, taking amorphous PCL as reference for this evaluation).

The thermal, thermo-mechanical and mechanical properties of the networks were investigated by differential scanning calorimetry (DSC), dynamic mechanical analysis (DMA) and mechanical testing.

Preliminary DSC tests were carried out on a DSC Q100 (TA Instruments) by performing heating/cooling/heating scans at 2 °C min^{-1} on about 8 mg of material cut from the casted sheets, to identify the melting temperature,T_m (on the 2nd heating scan), the crystallization temperature, T_c, and the enthalpies at melting and at crystallization, ΔH_m and ΔH_c, respectively. The thermal region covered ranges between $T_c - 50$ °C and $T_m + 40$ °C, approximately, and thus −50 / 65 °C, −40 / 70 °C and −20 / 90 °C for PCLSG 2, PCLSG 3 and PCLSG 10, respectively. The degree of crystallinity was calculated as the ratio between the measured ΔH_m (on the 2nd heating scan) and the specific melting enthalpy for 100% PCL crystalline phase, equal to 134.9 J g^{-1} [40].

DMA tests were performed under tensile configuration by means of the dynamic mechanical analyzer (DMA Q800, TA Instruments) on rectangular strips (gauge length: about 10 mm, cross-section: approximately 5 × 0.2 mm^2) subjected to an oscillating displacement amplitude of 15–30 μm at 1 Hz. The thermal ramp employed a cooling/heating history at a rate of 2 °C min^{-1} covering the temperature region between $T_c - 50$ °C and $T_m + 40$ °C, approximately, for each system.

Mechanical testing was performed under tensile conditions above the melting temperature, at about $T_m + 40$ °C on the rectangular strips at a rate of 0.05 N min^{-1} by using the dynamic mechanical analyzer.

Additional DSC tests were performed under two more complex thermal or thermo-mechanical histories.

The first thermal history consisted of introducing, after the typical heating-cooling-heating scans performed between $T_c - 50$ °C and $T_m + 40$ °C, a heating step up to a temperature $T_{isothermal}$ equal to either $T_m - 2$ °C or T_m, that was kept constant for 10 min, followed by cooling down to $T_c - 50$ °C and by heating up to $T_m + 40$ °C as the last heating run. These tests were performed at the same rate of 2 °C min^{-1} of the preliminary DSC tests and they were intended to study the thermal response on the crystallization and melting behavior after an isothermal step in proximity of the melting temperature, acting as an 'annealing' treatment.

In the second thermo-mechanical history, the thermal analysis was carried out on about 5 mg of materials cut from a rectangular strip which underwent a preliminary programming by means of the DMA Q800. In detail, the specimen was heated at $T_m + 40$ °C, deformed up to 30% of strain and cooled under fixed stress conditions (by keeping the load constant) down to $T_c - 50$ °C. Afterwards, the specimen was unloaded, heated under quasi-stress free conditions up to a certain separation temperature T_{sep}, and quasi-stress free cooling at 2 °C min^{-1} was performed down to $T_c - 50$ °C. At this point, the sample was quickly moved to a refrigerator at −20 °C prior to the DSC testing, which consisted of heating/cooling/heating scans at a rate of 2 °C min^{-1} in the thermal region $T_c - 50$ °C and $T_m + 40$ °C.

2.3. Two-way shape memory testing

The two-way shape memory response of the materials under different experimental protocols was studied by means of the dynamic mechanical analyzer under tensile configuration on rectangular strips (gauge length: 10 mm, cross-section: 5 × 0.2 mm^2) cut from the casted sheets.

The two-way shape memory response under stress conditions was evaluated by first applying a pre-stretch equal to 20% to the specimens above their melting temperature, at $T_m + 40$ °C; then, by keeping the corresponding applied load constant, the specimen was cooled well below T_c (down to $T_c - 50$ °C) and heated again up to $T_m + 40$ °C, at a rate of 5 °C min^{-1}.

The two-way shape memory testing under stress-free conditions was carried out by purposely designing two testing protocols.

In the first protocol, the effect of the so-called separation temperature, T_{sep}, on the reversible stress-free cycle was investigated according to the following thermo-mechanical history: (i) heating at $T_m + 40$ °C and application of a tensile pre-stretch of 20% (loading rate: $2{\cdot}10^{-2}$ N min^{-1}); (ii) cooling to $T_c - 50$ °C at 5 °C min^{-1} under the applied stress; (iii) unloading to a moderate load equal to 0.01 N, so to keep the sample in tension; (iv) heating to T_{sep} (heating rate was set to at 5 °C min^{-1}, and reduced to 0.5 °C min^{-1} when approaching T_{sep}); (v) at T_{sep}, cooling under quasi-stress free conditions at 2 °C min^{-1} well below T_c; (vi) repetition of steps (iv) and (v) for several times to explore various values of T_{sep}; (vii) final heating up to $T_m + 40$ °C at 5 °C min^{-1}. The explored values of T_{sep} depend on the material and are reported in the Results section.

In the second protocol, the effect of the pre-strain ε_{appl} on the reversible stress-free cycle was investigated with the following protocol: (i) heating at $T_m + 40$ °C and application of a tensile pre-strain, ranging from 5% to 40%, at a loading rate of 2×10^{-2} N min^{-1}; (ii) cooling down to $T_c - 50$ °C at 5 °C min^{-1} under the applied stress; (iii) unloading down to a small load equal to 0.01 N; (iv) heating to T_{sep} (heating rate was set to at 5 °C min^{-1}, and reduced to 0.5 °C min^{-1} when approaching T_{sep}); (v) at T_{sep}, cooling under quasi-stress free conditions at 2 °C min^{-1} well below T_c; (vi) heating under quasi-stress free conditions at 2 °C min^{-1} up to $T_m + 40$ °C.

The reversible stress-free cycle was also measured under flexural conditions by first deforming a rectangular strip (~20 mm long, ~5 mm wide, ~0.5 mm thick) at about $T_m + 40$ °C into a U-shaped bar and fixing it under the deformed shape by cooling down to −25 °C. Afterwards, two temperature-controlled baths were set up, one of them brought to a low temperature, T_{low}, equal to about 5 °C, and the other one to a high temperature, T_{sep}, whose value depends on the material and falls in a range around the melting temperature. T_{sep} was maintained by means of a cryostat (Thermo Haake C10 K20 Refrigerated Circulator Cryostat). The programmed U-shaped sample was then immersed and equilibrated in the

T_{sep} bath and later moved to the T_{low} bath. This cycle of immersion in the T_{sep} and T_{low} baths was repeated several times, each time increasing of about 1 °C the T_{sep} value, until reaching complete melting of the material. During the test, shape changes were recorded by means of a camera (Nikon D700) placed above the sample and the pictures were processed with a software (ImageJ) to measure the changes in the angle between the two arms of the sample. The PCLSG 2 tubular sample was also tested under similar conditions after deforming and fixing it in a six-arm star shape [26]. The sample in its six-arm star configuration was placed repeatedly in a T_{sep} and T_{low} bath, each time increasing the T_{sep} of about 1 °C until reaching complete melting. The temperature of both temperature-controlled baths was continuously monitored and recorded with a thermocouple placed near the sample.

3. Results and discussion

3.1. Materials characterization

The poly(ε-caprolactone) based networks PCLSG 2, PCLSG 3 and PCLSG 10 were successfully synthesized and crosslinked via a sol–gel approach. The various systems were obtained starting from hydroxyl-terminated PCL with different molecular weight, later reacted to provide triethoxysilane termination and finally through a sol–gel reaction, to provide a crosslinked structure where silica-like domains act as crosslinking points among the PCL chains, as shown in scheme 1. An extensive physico-chemical characterization of these materials is reported elsewhere [21, 24].

The presence of a semicrystalline network is of paramount importance in determining the two-way shape memory effect. The crosslinks provide the network structure that promotes the complete recovery of the deformation during the one-way shape memory cycle and they allow to design the reversible deformation for the two-way shape memory effect along the crystallization and melting regions of the materials without a loss of cohesion in the material. The crosslink density can also be leveraged as a tailoring variable, as it induces changes in the crystalline phase and in the thermal regions of melting and crystallization. Therefore, thermal analysis by DSC for the investigation of melting and crystallization was performed and the results are plotted in figure 1 and summarized in table 1.

All the networks regardless of the starting molecular weight of the precursors showed melting and crystallization transitions. As the molecular weight of the precursors increased, the melting and crystallization temperature of the materials increased, as well as the degree of crystallinity.

The effect of melting and crystallization processes on material mechanical response were also investigated by DMA. Figure 2 shows the storage modulus evolution along the temperature for the three materials along a cooling-heating cycle carried out from a temperature above T_m to one well below T_c of the specific system investigated. An evaluation of the value of the storage modulus at different temperatures is also provided in table 2. The change in storage modulus is about two orders of magnitude between the rubbery plateau (at

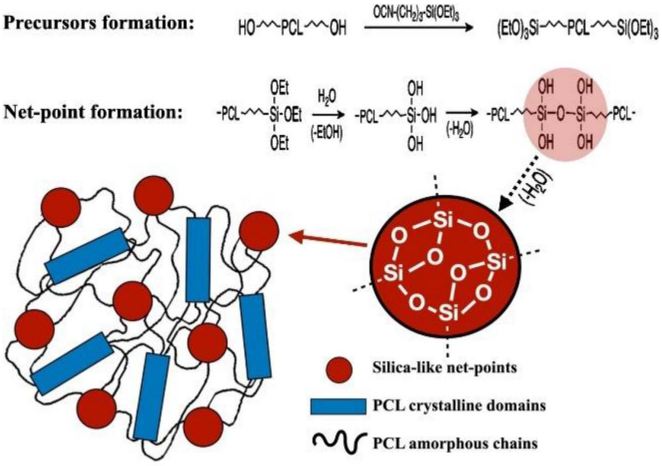

Scheme 1. Reaction scheme and the resulting macromolecular structure of the semicrystalline PCL networks.

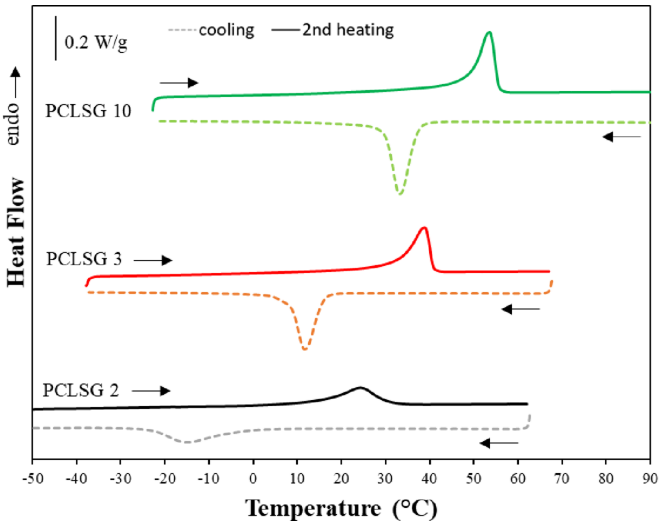

Figure 1. DSC cooling and 2nd heating run traces (dashed and continuous line, respectively) for PCLSG 2, PCLSG 3 and PCLSG 10.

temperatures greater than T_m) and the glassy plateau (at temperatures lower than T_c), and the material with the lowest molecular weight of the precursor (*i.e.* PCLSG 2) has the highest storage modulus in the rubbery plateau.

The rubber-like plateau of the storage modulus reached when melting is completed indicates the presence of a crosslinked network whose crosslinked density can be initially evaluated by equation (3)

$$E = 3\nu RT \tag{3}$$

where E is the material modulus in the rubbery region, here approximated by the value of the storage modulus in the rubbery plateau, R is the universal gas constant, T is the absolute temperature, and ν is the crosslinking density defined as moles per unit volume.

Table 1. Thermal properties of the networks from DSC analysis and results from swelling experiments. The degree of crystallinity χ_c was calculated considering the specific melting enthalpy for 100% PCL crystalline phase equal to 134.9 J g^{-1} [40]. The crosslink density was evaluated by using equation (3).

	T_c (°C)	T_m (°C)	ΔH_m (J g^{-1})	χ_c (%)	Degree of swelling (g g^{-1})	Gel content (%)	Crosslink density (mol cm^{-3})
PCLSG 2	−15	24	28.2	20.9	2.0 ± 0.2	94.5 ± 0.2	4.4×10^{-4}
PCLSG 3	12	39	36.2	26.9	3.0 ± 0.3	90.7 ± 0.2	1.3×10^{-4}
PCLSG 10	33	54	51.6	38.2	4.0 ± 0.2	92.2 ± 0.8	0.6×10^{-4}

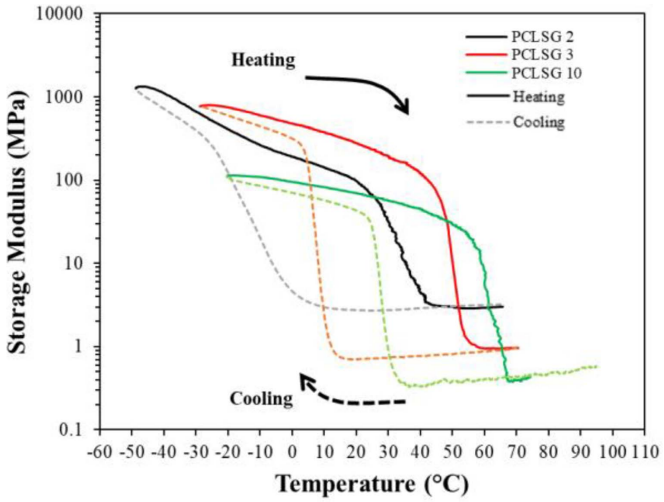

Figure 2. Storage modulus as a function of temperature upon cooling-heating cycle from above T_m to below T_c of PCLSG 2, PCLSG 3 and PCLSG 10. Solid line represents the heating curve and the dashed line represents the cooling curve for each material.

Table 2. Evaluation of the storage modulus (*E*') of the materials along the DMA cooling and heating traces for various temperatures.

	Cooling trace		Heating trace	
	E' at T_c[a] −15 °C (MPa)	*E*' at T_c[a] (MPa)	*E*' at T_m[b] (MPa)	*E*' at T_m[b] + 15 °C (MPa)
PCLSG 2	605.7	172.7	37.1	3.2
PCLSG 3	432.1	73.5	60.3	1.0
PCLSG 10	55.0	9.1	9.9	0.4

[a] T_c identified as the inflection point of the cooling trace, equal to −22 °C for PCLSG 2, 6 °C for PCLSG 3, 27 °C for PCLSG 10.
[b] T_m identified as the inflection point of the heating trace, equal to 29 °C for PCLSG 2, 46 °C for PCLSG 3, 59 °C for PCLSG 10.

From equation (3) the materials' crosslink density was estimated, and the values obtained are reported in table 1. As expected, materials obtained from lower molecular weight precursors (PCLSG 2 and PCLSG 3) have higher crosslink density than the one from the higher molecular weight precursor (PCLSG 10). In fact, for lower molecular weights of the precursor, the chain length between crosslinks is shorter compared to that of precursors with higher molecular weight, resulting in a higher density of crosslinks. Results of swelling experiments confirmed a lower degree of swelling for PCLSG 2 and PCLSG 3 compared to PCLSG 10, hence a higher crosslink density compared to PCLSG 10.

Tensile tests performed in the rubbery region (i.e. T_m + 40 °C for each system) allowed to investigate the extensibility of these networks which is another important variable when designing shape memory cycles. Results are reported in figure 3, showing that the less crosslinked network (PCLSG 10) is not only the most compliant but also the most extensible one. However, also PCLSG 2, which is the network with the highest crosslink density, allows for a significant tensile deformation (around 40%) before failure.

3.2. *Two-way shape memory results*

The materials were first tested with an ad hoc thermo-mechanical protocol employed to measure the stress-driven two-way shape memory effect, with the specific aim to investigate the stress-driven elongation during crystallization and the capability of recovering the deformation during heating under

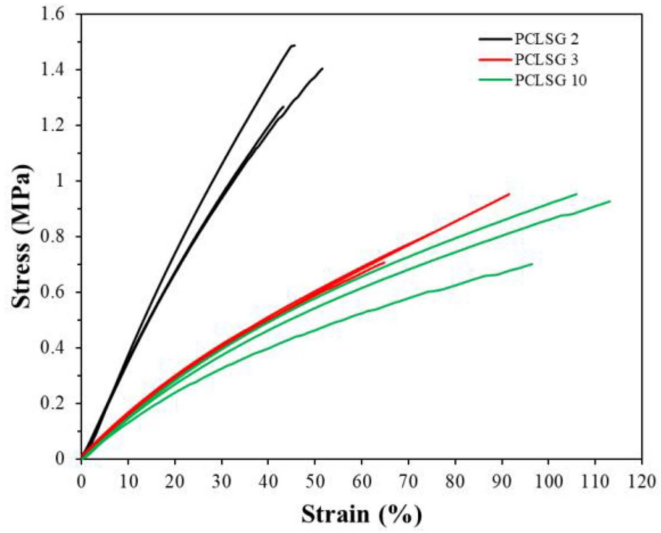

Figure 3. Stress-strain curves carried out until failure at about $T_m + 40$ °C, on PCLSG 2, PCLSG 3 and PCLSG 10.

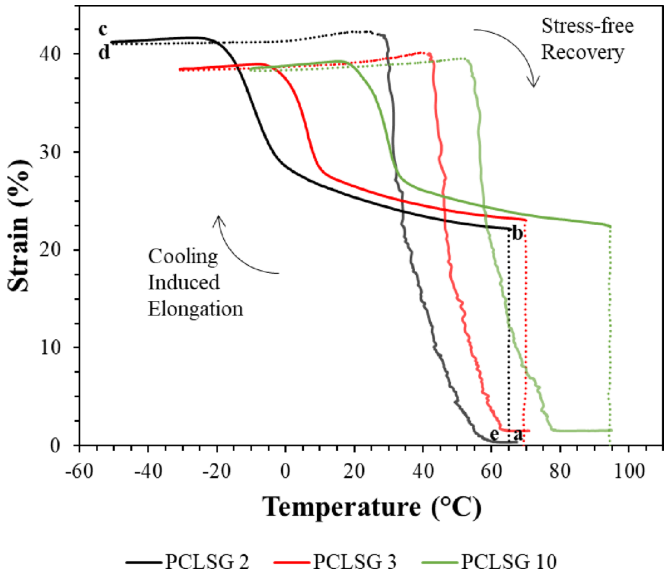

Figure 4. Strain vs. temperature in two-way shape memory tests for systems PCLSG 2, PCLSG 3 and PCLSG 10: cooling under-stress driven condition, followed by stress-free recovery.

stress-free conditions. Strain versus temperature curves measured in these experiments are reported in figure 4.

First, the samples were heated above the melting region, between 65 °C to 95 °C depending on the material T_m, and deformed up to a tensile strain equal to 20% (a → b); by keeping the corresponding load applied, the samples were cooled below their crystallization temperature (b → c), displaying an elongation induced by crystallization; then, they were unloaded (c → d), and heated at a controlled heating rate above the melting temperature to trigger strain recovery (d → e). In order to compare the two-way shape memory behavior of the three materials, which are characterized by different stiffness at the deformation temperature (figure 3, table 2), the same nominal strain (equal to 20%) was applied, and this was reached under various load (equivalent to a tensile stress of about 740 kPa for PCLSG 2, 320 kPa for PCLSG 3, and 300 kPa for PCLSG 10). The crystallization-induced elongation (CIE) occurs for all the networks in correspondence of the sharp strain increase in the characteristic thermal region of crystallization for each network. The amount of deformation achieved at the end of cooling was quantified with the parameter called actuation magnitude (AM) defined in equation (4):

$$\text{actuation magnitude, AM}\,(\%) = \varepsilon_c - \varepsilon_b \tag{4}$$

where ε_c represents the strain at the end of cooling and ε_b the pre-strain applied before cooling.

AM resulted to be very similar among the three networks in terms of the amount (e.g. 20% approximately), while the factor that differentiates the materials is the thermal region in which the majority of the CIE is happening. Interestingly, all these systems can achieve a significant deformation under tensile conditions, which can be almost completely (more than 90%) recovered upon melting. This can be evaluated by comparing the deformation recovered during melting (d → e) to the deformation achieved because of the mechanical stretch imposed and the CIE (a → b → c).

The motivation for such an effect with a significant deformation upon cooling can be sought in the structural evolution of the material taking place in this thermo-mechanical cycle. When the molten network is pre-stretched and cooled down under the applied load, crystal formation occurs in the crystallization region together with a relaxation of the polymer. To maintain mechanical equilibrium, given that the external load applied remains constant, the polymer further stretches leading to this CIE. Such an elongation, although being based on a structural evolution, can be recovered when melting the crystals and restoring the rubbery phase.

One of the strategies recently proposed in the literature to remove the external mechanical load for such an effect regards the possibility of substituting it with an internal stress acting likewise as the driving force for the elongation. This was hypothesized possible by adopting a multi-phase polymer system in which one phase can be the driving force while the other undergoes the thermal transitions [16], or by using a semicrystalline homopolymer network with a broad enough melting region that allows to use part of the crystals as the actuator domain cyclically crystallizing and melting and the other part of the crystals as the internal driving force acting as the so-called skeleton domain [31, 41, 42].

For these systems melting and the concomitant strain recovery occur as a single process distributed along the temperature scale on a 20 °C–30 °C region. Therefore, in absence of two distinguished, or broadly distributed, crystalline domains, the fairly homogeneous crystalline phase has to be partly used as skeleton and as active domains.

To test this behavior, the material, heated above T_m and stretched up to a given strain, was subjected to cooling under

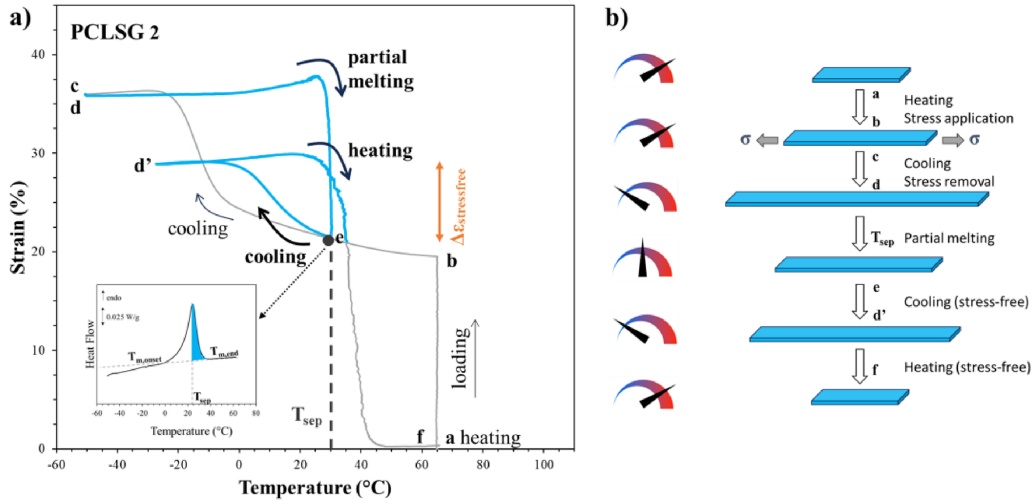

Figure 5. (a) Typical stress-free two-way response for system PCLSG 2; insert: schematic description of the correspondence of partial melting in DSC diagrams and partial recovery in shape memory tests. (b) Schematic representation of the macroscopic change of the specimen during the testing protocol.

constant load promoting a further elongation, as in a traditional two-way shape memory test under fixed stress; however, after this, the load was removed and the material was heated at a given separation temperature, T_{sep}, to promote partial melting of the crystalline phase and causing a concomitant partial recovery; finally the material was subjected to a cooling-heating cycle between T_{sep} and a temperature below T_c. The response is an elongation-contraction cycle under no applied load, that may be considered as a reversible two-way effect. Such a reversible behavior during the final cooling-heating cycle may be considered as a result of the preceding thermo-mechanical history, which acts as a sort of training of the material for the self-standing response.

The aim of the stress-free two-way shape memory testing was indeed here addressed to understand and design these two components for these systems, and to better highlight the proper value of T_{sep} to emphasize the elongation-contraction behavior. To do so, a specific thermo-mechanical protocol was employed to cyclically promote stress-free elongation contraction for various, progressively increasing, values of T_{sep}. The protocol together with a schematics of the macroscopic shape changes occurring is represented in figures 5(a) and (b).

The material was first elongated by applying a fixed load after heating (a $\rightarrow$ b) and by maintaining it constant during the test; this allowed to activate the typical CIE under applied stress (b $\rightarrow$ c); after this, the load was removed (c $\rightarrow$ d; c and d overlap) and the material was heated until a specific T_{sep} value, promoting partial melting, and partial recovery (d $\rightarrow$ e); if cooling below crystallization is induced, the stress-free elongation cycle is observed and may be quantified (e $\rightarrow$ d'). By repeating the process of partial melting and cooling and progressively increasing T_{sep}, several elongation-contraction cycles without external load applied can be observed along cooling-heating, until the whole available crystalline fraction is melted and the recovery is completed (point f). This effect was observed for all the materials tested to different extents.

The effect is considered to be due to a frozen stress arising between the crystal structure and the surrounding polymer chains; such stress, still present after partial melting, is believed to act as an internal driving force for the two-way shape memory effect of the surrounding structure.

According to this interpretation, it is clear that an important parameter is the extent of this partial melting, since it may have an effect on the internal stress provided and in the crystal fraction that may be reformed in the two-way effect. For this reason, we explored how the material behaved for various degrees of partial melting, here accounted as ratio between the partially recovered strain and the maximum strain.

The results recorded are plotted as strain versus temperature curves in figures 6(a)–(c) for PCLSG 2, PCLSG 3 and PCLSG 10, respectively, in a cyclic experiment done with the DMA, where the T_{sep} was systematically increased form cycle to cycle, so to progressively reduce the amount of residual crystallinity. Interestingly, the reversible deformation can be obtained over a large interval of temperature depending on the polymer precursor, ranging from 30 °C–35 °C, 40 °C–45 °C and 58 °C–62 °C, for PCLSG 2, PCLSG 3, and PCLSG 10, respectively.

All the systems showed that a partial melting of the crystalline state is required in order to actuate the two-way response. In fact, both PCLSG 2 and PCLSG 10 displayed no shape changes, other than those related to thermal expansion-contraction, for the lowest value of T_{sep} explored, where all the crystals are still intact (marked with the symbol * in figures 6(a) and (c). As T_{sep} increases, an overall larger cyclic elongation-contraction is achieved, and it disappears only after full melting. However, in the case of PCLSG 10 the extent of the elongation-contraction cycle with T_{sep} is less evident than that for both PCLSG 2 PCLSG 3.

The stress-free reversible deformation for each cycle, $\varepsilon_{rev,}$ was quantified as the difference in elongation between the end of cooling (points d') and the end of partial melting

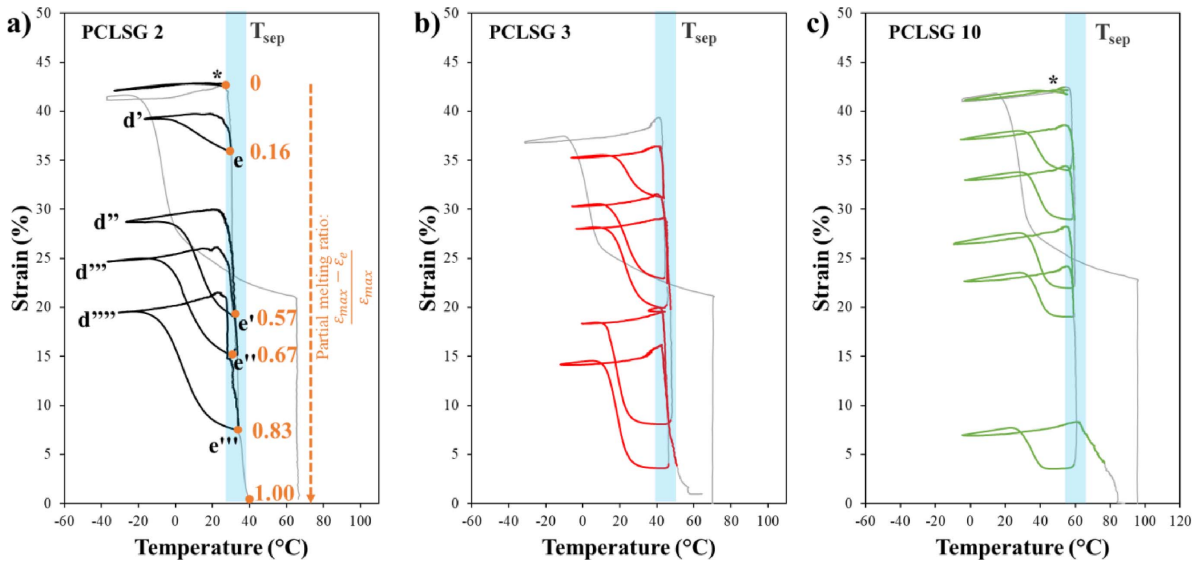

Figure 6. Effect of the separation temperature, T_{sep}, on the stress-free two-way shape memory response for (a) PCLSG 2, (b) PCLSG 3, and (c) PCLSG 10. The multiple cooling-heating cycles are highlighted with the letters e–d' in panel (a) as an example. Cycles which do not result in any elongation-contraction changes, other than those related to thermal expansion-contraction, are marked with an asterisk (*) in panel (a) and panel (c).

(points e, e', and subsequent ones) and plotted as a function of the partial recovery ratio defined as per equation (5):

$$\text{partial recovery ratio} = \frac{\varepsilon_{max} - \varepsilon_e}{\varepsilon_{max}} \tag{5}$$

where ε_{max} corresponds to the maximum strain observed in the whole test and ε_e is the strain due to the partial melting when heating at the given T_{sep} and measured in correspondence of the beginning of the subsequent cooling step. The partial recovery ratio is in fact representative of partial melting and it may be considered proportional to the amount of residual crystallinity (the skeleton phase).

The stress-free cooling induced elongation, $\Delta\varepsilon_{stress\text{-}free}$, obtained for the various values of T_{sep}, is displayed as a function of the corresponding partial recovery ratio in figure 7 for the three materials.

Both PCLSG 2 and PCLSG 3 showed a very similar response, showing a linear increase of the stress-free cooling induced strain upon increasing the partial recovery ratio ($R^2 > 0.96$); only above a partial recovery ratio equal to 0.8, i.e. at almost complete melting, a decreasing trend is suggested until, at full melting, no more deformation can be actuated and recovered. PCLSG 10 showed an increasing dependence of the stress-free cooling induced strain only up to a value of partial recovery ratio equal to 0.4, approximately, after which the elongation becomes less and less as the partial recovery ratio increases; in these latter conditions, the elongation process becomes less and less effective, probably due to a reduced stress in the crystal structure for this low crosslinked system. This representation is very useful to draw the design space for this actuation and obtain the optimal actuation conditions for each material under these experimental conditions.

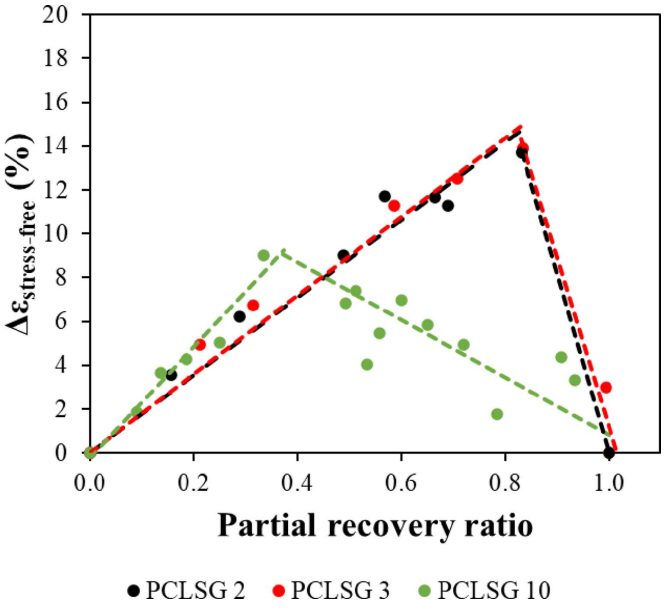

Figure 7. Stress-free cooling induced elongation, $\Delta\varepsilon_{stress\text{-}free}$, as a function of the corresponding partial recovery ratio for the three systems PCLSG 2, PCLSG 3 and PCLSG 10. The dependence of the stress-free cooling induced elongation can be approximated with various fitting lines (dashed lines: best fit linear regression on the increasing and decreasing parts of the trend).

3.3. Thermal characterization after isothermal annealing

In an attempt to gain more information on the evolution of the residual crystalline phase during these thermo-mechanical cycles, DSC analyses were carried out by applying an additional isothermal annealing step at different temperatures close to the melting peak of the network. This is aimed at simulating

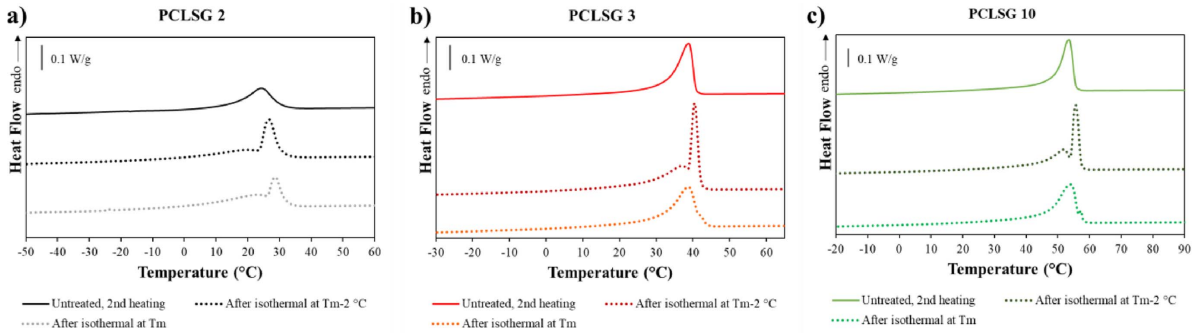

Figure 8. DSC traces for the untreated material (solid line), the material after an annealing thermal treatment at $T_m - 2$ °C (dotted line, dark color) and the material after an annealing thermal treatment at T_m (dotted line, light color) for (a) PCLSG 2, (b) PCLSG 3 and (c) PCLSG 10.

Table 3. DSC results for PCLSG systems after an annealing thermal treatment at $T_{isothermal}$ equal to $T_m - 2$ °C or to T_m. The degree of crystallinity χ_c was calculated considering the specific melting enthalpy for 100% PCL crystalline phase equal to 134.9 J g^{-1} [40].

	T_m (°C)	$T_{isothermal}$ (°C)	$T_{sub\text{-}peak}$ (°C)	T_{peak} (°C)	ΔH_m (J g^{-1})	χ_c (%)
PCLSG 2	24	22 (*i.e.* $T_m - 2$ °C)	20	27	34.6	25.6
		24 (*i.e.* T_m)	23	29	34.7	25.7
PCLSG 3	39	37 (*i.e.* $T_m - 2$ °C)	37	41	50.3	37.3
		39 (*i.e.* T_m)	—	39	41.6	30.8
PCLSG 10	54	52 (*i.e.* $T_m - 2$ °C)	52	56	52.3	38.8
		54 (*i.e.* T_m)	57	54	52.4	38.8

the crystalline phase evolution during the two-way shape memory cycles when reaching a separation temperature T_{sep} equal to T_m or $T_m - 2$ °C prior to the stress-free cooling/heating cycle. The resulting heating thermal scans after isothermal annealing and cooling are shown in figure 8 compared to the DSC scan of the untreated materials shown in figure 1.

Interestingly, after the isothermal holding and cooling, the melting process appears to be changed compared to the untreated material (figure 8). In fact, for annealing at $T_m - 2$ °C, the endothermal peak changes shape splitting in a more pronounced and narrower peak at high temperature associated with the formation of more regular crystals, accompanied by a shoulder, typically at lower temperatures. In some traces, the shoulder to the left of the main peak could be considered as a secondary sub-peak (figure 8). To note, the shoulder is located close to the temperature at which the annealing was performed, whereas the main peak shifts to higher temperature, indicating the effect of the annealing in thickening the unmelted crystals (table 3). By contrast, after annealing at T_m, only PCLSG 2 still displays the low-temperature sub-peak, whereas PCLSG 3 and PCLSG 10 show a more homogenous melting peak with only a less relevant shoulder at high temperature.

On the network system with the highest melting temperature, far from room temperature (PCLSG 10), it was also possible to perform DSC on a sample subjected to the shape memory cycle in the DMA and removed from the clamp after the obtainment of the stress-free CIE by cooling at low temperature, as outlined in figure 9.

Compared to the untreated material, the sample after CIE under stress-free conditions shows a narrower melting process with a higher temperature of the peak. Interestingly, compared to the scans of the isothermally annealed samples, the melting peak overlaps with the highest of the two sub-peaks of the isothermally annealed samples. The results in figures 8 and 9 suggest that the partial melting in the shape memory cycles may act similarly to the annealing treatment in promoting a broader crystal melting interval. The unmelted phase during the shape memory cycle could act as a skeleton, while the remaining crystals melt and crystallize at each cycle, accompanying the specimen strain evolution in doing so. Other studies have also contemplated the possibility of self-nucleation and annealing of crystals as a beneficial factor for achieving stress-free reversible shape memory effect [38].

3.4. Comparison between the stress-driven and the stress-free two-way shape memory response

Another important parameter that is expected to affect the two-way response under stress-free conditions regards the pre-stretch, as potentially allowing to change the amount of internal stress. Initial programming parameters are in fact known to affect the structural evolution of the material under stress-driven two-way shape memory conditions [23], and especially the pre-strain imposed during deformation in the rubbery plateau. Thus, the dependance of the reversible deformation of the pre-strain was investigated by varying the tensile pre-strain in the range 5%–45% and measuring the

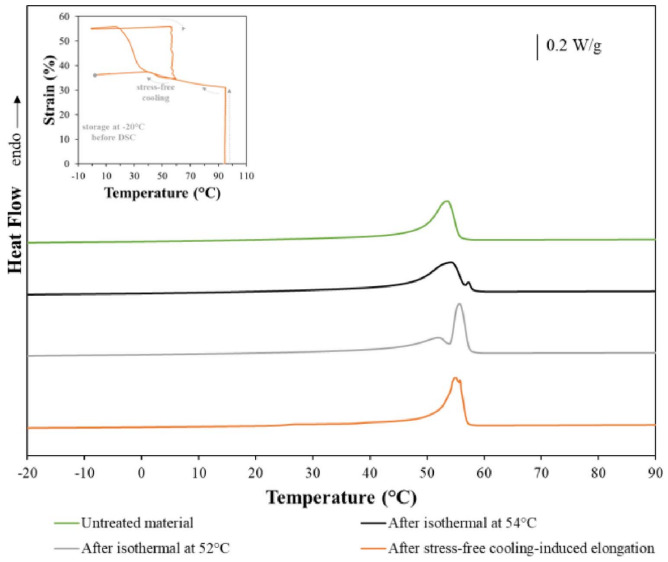

Figure 9. DSC traces for PCLSG 10 under various conditions: untreated material (green solid line, 2nd heating); material subjected to isothermal annealing at $T_m = 54$ °C (black solid line); material subjected to isothermal annealing at $T_m - 2$ °C $= 52$ °C (grey solid line); material after the stress-free cooling induced elongation (orange solid line). Insert: thermomechanical cycles used to prepare the material obtained by stress-free CIE.

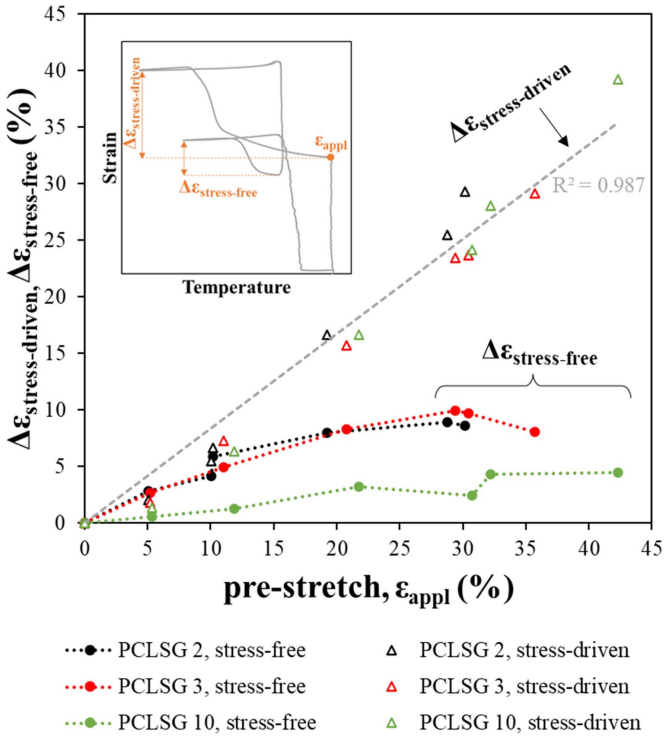

Figure 10. Effect of the pre-stretch amplitude on the two-way shape memory response under stress-free (filled circles) and stress-driven conditions (empty triangles). The grey dashed line represents the linear correlation between the amplitude of the stress-driven deformation and the amplitude of the pre-stretch.

two-way response, according to the usual protocol at a given T_{sep} (i.e. ~30 °C for PCLSG 2, ~43 °C for PCLSG 3, ~59 °C for PCLSG 10). The results are reported in figure 10 where a comparison between the reversible deformation obtained under stress-driven and stress-free conditions after various pre-strain is shown.

A strong linear correlation between the amount of pre-strain and the reversible deformation under stress-driven conditions is suggested when grouping together all the materials (experimental points shown with empty triangles in figure 10), independently from the material structure. The results under stress-free conditions clearly show that the stress-free effect is smaller in amplitude with respect to the stress-driven one, especially for high pre-strains involved (greater than 15%, approximately), and it also tends to saturate to a steady state value at higher strain level. Furthermore, the stress-free reversible strain is confirmed to be greater and more effective for networks with a higher crosslink density, which can reach up to 10% reversible strain under stress-free conditions (PCLSG 2 and PCLSG 3).

While the stress-driven two-way shape memory response can provide significant reversible strain, which may be useful for a large reversible deformation of a structure, the requirement of keeping the load applied throughout the thermal cycling can be limiting and difficult to be maintained. Furthermore, a tensile load is usually used, resulting in a cyclic contraction-extension, and this limits other deformation modes.

The possibility of external stress-free actuation can be of paramount importance for actuators and untethered devices that are not connected to joints and other sections of a structure that could provide a constant load. Another advantage of the stress-free two-way shape memory effect is that the maximum reversible deformation found for PCLSG 2 and PCLSG 3 can be further amplified if exploring flexural conditions as shown in figure 11. Here, I-shaped bars were initially deformed and fixed into a U shape. The U-shaped bars were placed in a heated bath to allow for partial recovery/melting and subsequently moved to a cold bath to trigger the cooling-induced deformation under stress-free conditions. Heating–cooling cycles determine an opening-closing effect of the U-shaped bar, showing a more open configuration at the higher temperature, and a reversible closing when cooling at the lower temperature (figure 11(a)). Upon placement in the thermal baths, the samples underwent shape changes after thermal equilibration at the bath temperature; for these thin samples, shape change occurred in less than 30 s. An evaluation of the reversible angle, $\Delta\alpha_{rev}$, defined as the difference between the angle of the U-shaped bar arms at the higher temperature, i.e. T_{sep}, and that of the arms after cooling-induced deformation, is shown in figure 11(b). Interestingly, the system PCLSG 2 shows a maximum $\Delta\alpha_{rev}$ value close to 70° for a T_{sep} value of 25 °C.

The large angular deformation possible is shown as an example in figure 11(a), as they might be relevant for the case of hinges of a multi-component, multi-material system, where the reversible deformation, even though localized, can have a huge overall impact on a structure. For example, grippers with

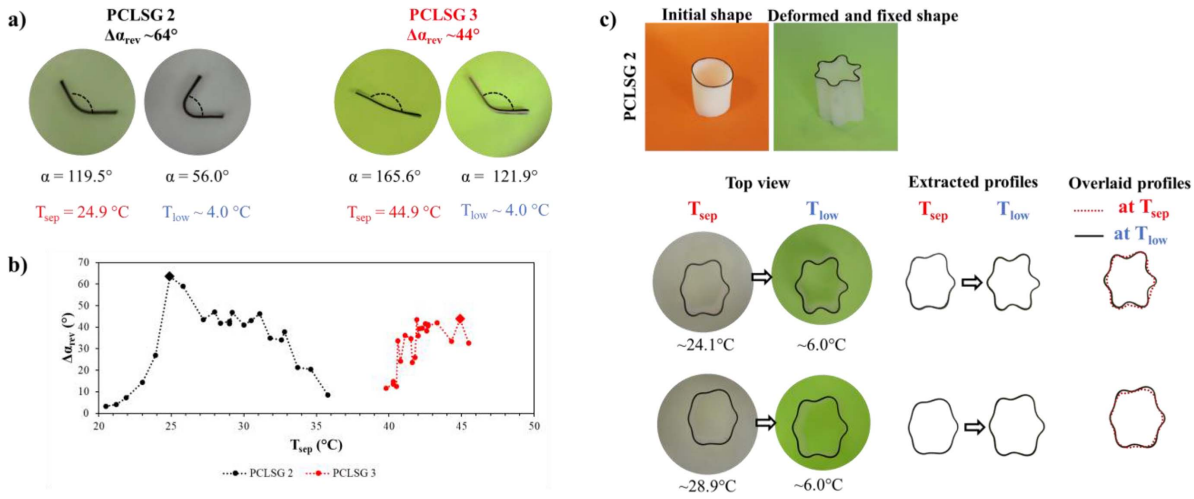

Figure 11. (a) Stress-free reversible opening-folding effect for systems PCLSG 2 and PCLSG 3. (b) Evaluation of the reversible angle for a U → I -bar deformation as a function of increasingly greater T_{sep} during cyclic testing for PCLSG 2 (black markers) and PCLSG 3 (red markers). The bigger diamond-shape marker indicates the temperature and reversible angle for which the pictures in panel a) are reported. Bars are about 20 mm long. (c) Deformation of a tubular structure (outer diameter of 25 mm) made of PCLSG 2 into a six-arm star shape (first row). The star profile is recorded (top view) during subsequent immersion in T_{sep} and T_{low} baths. The star profile is isolated from the background and the relevant profiles are overlaid for better visualizing the reversible shape changes.

fingers made of reversible SMPs could be especially useful for an on-demand soft capturing/releasing of an object. In addition to gripping tasks, actuators made of these materials could be used in soft robotics for locomotion purposes. In fact, the on-demand and sequential bending of multiple hinges can be used for achieving self-rolling in 3D structures [43]. More complex deformation may also be possible, for example in the case of the tubular structure deformed into a star profile, as shown in figure 11(c). When partially recovering/melting the star profile, it turns closer to the initial circular cross-section, however, upon immersing into cold baths, the star profile geometry returns to be more prominent. Furthermore, by a proper selection of the molecular weight of the polymer precursor, it is possible to tune the actuation temperature to accommodate various potential applications, including triggering at a temperature close to that of human body. This approach, based on using homopolymer with broad melting region, tunable based on the polymer precursor, is thus promising in the field of 3D printing of two-way SMPs, i.e. 4D printing, for reversible and self-standing actuators, which are currently being explored with many various approaches [44–48].

4. Conclusion

Semicrystalline polymeric networks based on poly(ε-caprolactone) crosslinked by a sol–gel approach resulted to have optimal macromolecular characteristics for the achievement of both stress-driven and stress-free two-way shape memory effect. The selection of the polymer precursor molecular weight allowed to tune the physical and thermal properties of the networks which are responsible for the shape memory effect. All crosslinked networks showed a melting process which can be leveraged during the thermo-mechanical programming of the two-way shape memory effect. Under tensile conditions, when the actuation temperature of the cooling-heating cycle is located inside the melting region, the low-melting point crystals are forced to melt, crystallize and melt again, while the high-melting point crystals not affected by the temperature cycle can provide a driving force for stress-free reversible deformation with elongation (during cooling) and contraction (during heating).

The amplitude of the reversible deformation was found to be highly dependent on the fraction of crystalline domains available for the crystallization-melting cycle with the presence of an optimum condition across all the networks tested. A dependance on the tensile pre-stretch performed on the networks in their melting region as part of the programming of the materials was also demonstrated.

By changing these parameters, it was possible to obtain non-negligible values of reversible deformation under uniaxial conditions close to 15%. While these values are still lower compared to their counterparts obtained under the more traditional stress-driven conditions (showing a maximum around 40%), they may provide a significant effect that can be magnified under different conditions or as part of a multi-material structure. As an example, a stress-free reversible deformation with an appreciable effect was shown under flexural conditions, showing how these materials might be promising for applications as reversible actuators for the soft robotic and biomedical fields.

Data availability statement

The data that support the findings of this study are openly available at the following URL/DOI: https://zenodo.org/records/10995304 [49].

Acknowledgments

This work was partially supported by the INSTM Consortium through the project 'New materials and computational approaches for 4D printing'. The authors would like to acknowledge Metalpres Donati Spa (Passirano (BS), Italy) and Rubinetterie Bresciane Bonomi Spa (Gussago (BS), Italy). The authors thank Gabriele Gemmo for his kind help with the characterization of the materials.

ORCID iDs

Nicoletta Inverardi https://orcid.org/0000-0003-3550-9299
Maurizio Toselli https://orcid.org/0000-0003-3615-5728
Massimo Messori https://orcid.org/0000-0003-3598-4241
Giulia Scalet https://orcid.org/0000-0001-7683-566X
Ferdinando Auricchio https://orcid.org/0000-0002-3735-2400
Stefano Pandini https://orcid.org/0000-0003-2390-8495

References

[1] Delaey J, Dubruel P and Van Vlierberghe S 2020 Shape-memory polymers for biomedical applications *Adv. Funct. Mater.* **30** 1909047
[2] Melocchi A, Uboldi M, Cerea M, Foppoli A, Maroni A, Moutaharrik S, Palugan L, Zema L and Gazzaniga A 2021 Shape memory materials and 4D printing in pharmaceutics *Adv. Drug Deliv. Rev.* **173** 216–37
[3] Inverardi N *et al* 2021 Experimental and computational analysis of a pharmaceutical-grade shape memory polymer applied to the development of gastroretentive drug delivery systems *J. Mech. Behav. Biomed. Mater.* **124** 104814
[4] Uboldi M *et al* 2022 Expandable drug delivery systems based on shape memory polymers: impact of film coating on mechanical properties and release and recovery performance *Pharmaceutics* **14** 2814
[5] Liu Y, Du H, Liu L and Leng J 2014 Shape memory polymers and their composites in aerospace applications: a review *Smart Mater. Struct.* **23** 023001
[6] Scalet G 2020 Two-way and multiple-way shape memory polymers for soft robotics: an overview *Actuators* **9** 10
[7] Soleimanzadeh H, Rolfe B, Bodaghi M, Jamalabadi M, Zhang X and Zolfagharian A 2023 Sustainable robots 4D printing *Adv. Sustain. Syst.* **7** 2300289
[8] Lalegani Dezaki M and Bodaghi M 2023 Shape memory meta-laminar jamming actuators fabricated by 4D printing *Soft Matter* **19** 2186–203
[9] Khalid M Y, Arif Z U, Ahmed W, Umer R, Zolfagharian A and Bodaghi M 2022 4D printing: technological developments in robotics applications *Sens. Actuators* A **343** 113670
[10] Lendlein A and Kelch S 2002 Shape-memory polymers *Angew. Chem., Int. Ed.* **41** 2034–57
[11] Behl M and Lendlein A 2007 Shape-memory polymers *Mater. Today* **10** 20–28
[12] Leng J, Lan X, Liu Y and Du S 2011 Shape-memory polymers and their composites: stimulus methods and applications *Prog. Mater. Sci.* **56** 1077–135
[13] Wang K, Jia Y-G, Zhao C and Zhu X X 2019 Multiple and two-way reversible shape memory polymers: design strategies and applications *Prog. Mater. Sci.* **105** 100572
[14] Lendlein A and Gould O E C 2019 Reprogrammable recovery and actuation behaviour of shape-memory polymers *Nat. Rev. Mater.* **4** 116–33
[15] Pasini C, Inverardi N, Battini D, Scalet G, Marconi S, Auricchio F and Pandini S 2022 Experimental investigation and modeling of the temperature memory effect in a 4D-printed auxetic structure *Smart Mater. Struct.* **31** 095021
[16] Behl M, Kratz K, Zotzmann J, Nöchel U and Lendlein A 2013 Reversible bidirectional shape-memory polymers *Adv. Mater.* **25** 4466–9
[17] Behl M, Kratz K, Noechel U, Sauter T and Lendlein A 2013 Temperature-memory polymer actuators *Proc. Natl Acad. Sci.* **110** 12555–9
[18] Chung T, Romo-Uribe A and Mather P T 2008 Two-way reversible shape memory in a semicrystalline network *Macromolecules* **41** 184–92
[19] Hong S J, Yu W-R and Youk J H 2010 Two-way shape memory behavior of shape memory polyurethanes with a bias load *Smart Mater. Struct.* **19** 035022
[20] Zotzmann J, Behl M, Hofmann D and Lendlein A 2010 Reversible triple-shape effect of polymer networks containing polypentadecalactone- and poly(ε-caprolactone)-segments *Adv. Mater.* **22** 3424–9
[21] Paderni K, Pandini S, Passera S, Pilati F, Toselli M and Messori M 2012 Shape-memory polymer networks from sol–gel cross-linked alkoxysilane-terminated poly(ε-caprolactone) *J. Mater. Sci.* **47** 4354–62
[22] Messori M, Degli Esposti M, Paderni K, Pandini S, Passera S, Riccò T and Toselli M 2013 Chemical and thermomechanical tailoring of the shape memory effect in poly(ε-caprolactone)-based systems *J. Mater. Sci.* **48** 424–40
[23] Pandini S, Passera S, Messori M, Paderni K, Toselli M, Gianoncelli A, Bontempi E and Riccò T 2012 Two-way reversible shape memory behaviour of crosslinked poly(ε-caprolactone) *Polymer* **53** 1915–24
[24] Pandini S, Baldi F, Paderni K, Messori M, Toselli M, Pilati F, Gianoncelli A, Brisotto M, Bontempi E and Riccò T 2013 One-way and two-way shape memory behaviour of semi-crystalline networks based on sol–gel cross-linked poly(ε-caprolactone) *Polymer* **54** 4253–65
[25] Hao C, Wang K, Wang Z, Duan R, Liu H, Huang M, Liu W, He S and Zhu C 2022 Triple one-way and two-way shape memory poly(ethylene-co-vinyl acetate)/poly(ε-caprolactone) immiscible blends *J. Appl. Polym. Sci.* **139** 51426
[26] Pandini S *et al* 2014 Tailored one-way and two-way shape memory capabilities of poly(ε-caprolactone)-based systems for biomedical applications *J. Mater. Eng. Perform.* **23** 2545–52
[27] Saatchi M, Behl M, Nöchel U and Lendlein A 2015 Copolymer networks from oligo(ε-caprolactone) and n-butyl acrylate enable a reversible bidirectional shape-memory effect at human body temperature *Macromol. Rapid Commun.* **36** 880–4
[28] Inverardi N, Toselli M, Scalet G, Messori M, Auricchio F and Pandini S 2022 Stress-free two-way shape memory effect of poly(ethylene glycol)/poly(ε-caprolactone) semicrystalline networks *Macromolecules* **55** 8533–47
[29] Liang R, Yu H, Wang L, Amin B U, Wang N, Fu J, Xing Y, Shen D and Ni Z 2021 Triple and two-way reversible shape memory polymer networks with body temperature and water responsiveness *Chem. Mater.* **33** 1190–200
[30] Yang G, Liu X, Tok A I Y and Lipik V 2017 Body temperature-responsive two-way and moisture-responsive one-way shape memory behaviors of poly(ethylene glycol)-based networks *Polym. Chem.* **8** 3833–40
[31] Zhou J, Turner S A, Brosnan S M, Li Q, Carrillo J-M Y, Nykypanchuk D, Gang O, Ashby V S, Dobrynin A V and

Sheiko S S 2014 Shapeshifting: reversible shape memory in semicrystalline elastomers *Macromolecules* **47** 1768–76
[32] Qian C, Dong Y, Zhu Y and Fu Y 2016 Two-way shape memory behavior of semi-crystalline elastomer under stress-free condition *Smart Mater. Struct.* **25** 085023
[33] Hui J, Xia H, Fu Y, Qiu Y and Ni Q-Q 2020 Two-way reversible shape memory properties of benzoyl peroxide crosslinked poly(ethylene-co-vinyl acetate) under different stress conditions *Macromol. Mater. Eng.* **305** 1900825
[34] Hui J, Xia H, Chen H, Qiu Y, Fu Y and Ni Q-Q 2020 Two-way reversible shape memory polymer: synthesis and characterization of benzoyl peroxide-crosslinked poly(ethylene-co-vinyl acetate) *Mater. Lett.* **258** 126762
[35] Dolynchuk O, Kolesov I, Jehnichen D, Reuter U, Radusch H-J and Sommer J-U 2017 Reversible shape-memory effect in cross-linked linear poly(ε-caprolactone) under stress and stress-free conditions *Macromolecules* **50** 3841–54
[36] Meng Y, Jiang J and Anthamatten M 2015 Shape actuation via internal stress-induced crystallization of dual-cure networks *ACS Macro Lett.* **4** 115–8
[37] Fan L F, Rong M Z, Zhang M Q and Chen X D 2018 Dynamic reversible bonds enable external stress-free two-way shape memory effect of a polymer network and the interrelated intrinsic self-healability of wider crack and recyclability *J. Mater. Chem.* A **6** 16053–63
[38] Yuan W, Liu K, Zhou J, Ni L, Shan G, Bao Y and Pan P 2020 Stress-free two-way shape memory effects of semicrystalline polymer networks enhanced by self-nucleated crystallization *ACS Macro Lett.* **9** 1325–31
[39] Inverardi N, Pandini S, Gemmo G, Toselli M, Messori M, Scalet G and Auricchio F 2022 Reversible stress-driven and stress-free two-way shape memory effect in a sol-gel crosslinked polycaprolactone *Macromol. Symp.* **405** 2100254
[40] Miller R L 1992 *Polymer Handbook* ed J Brandrup, E H Immergut and E A Grulke (Wiley)
[41] Arricca M, Inverardi N, Pandini S, Toselli M, Messori M, Auricchio F and Scalet G 2024 Phenomenological modeling of the stress-free two-way shape-memory effect in semi-crystalline networks: formulation, numerical simulation, and experimental validation *Eur. J. Mech.* A **105** 105245
[42] Wang J, Zhang H, Lei J, Wu M, Liu W and Qu J-P 2022 Stress-free two-way shape-memory mechanism of a semicrystalline network with a broad melting transition *Macromolecules* **55** 10113–23
[43] Zhao Y, Peng K, Xi J, Shahab S and Mirzaeifar R 2022 Achieving multimodal locomotion by a crosslinked poly(ethylene-co-vinyl acetate)-based two-way shape memory polymer *Smart Mater. Struct.* **31** 015034
[44] Bonetti L, Natali D, Pandini S, Messori M, Toselli M and Scalet G 2024 4D printing of semi-crystalline crosslinked polymer networks with two-way shape-memory effect *Mater. Des.* **238** 112725
[45] Jiang Y, Leng Q Y, Yan Y, Ng E L L, Chee H L, Wang F, Chan S Y, Loh X J, Wang J and Chan B Q Y 2022 4D printing of single-network shape memory polyurethanes with two-way actuation properties *ACS Appl. Polym. Mater.* **4** 8574–83
[46] Li S *et al* 2023 4D printed thermoplastic polyamide elastomers with reversible two-way shape memory effect *Adv. Mater. Technol.* **8** 2202066
[47] Pasini C, Soreño Z V, Schönfeld D, Pretsch T, Constante G, Sadilov I and Ionov L 4D fabrication of two-way shape memory polymeric composites by electrospinning and melt electrowriting *Macromol. Rapid Commun.* **45** 2400010
[48] Chalissery D, Schönfeld D, Walter M, Ziervogel F and Pretsch T 2022 Fused filament fabrication of actuating objects *Macromol. Mater. Eng.* **307** 2200214
[49] Inverardi N, Toselli M, Messori M, Scalet G, Auricchio F and Pandini S 2024 Dataset for "Tailoring the stress-free two-way shape memory effect in sol-gel crosslinked poly(ε-caprolactone)-based semicrystalline networks" [Data set]. Zenodo (https://doi.org/10.5281/zenodo.10995304)